COLLAPSING CLOUD MODELS FOR BOK GLOBULES

KAREN R. VILLERE[1] AND DAVID C. BLACK
Space Science Division, NASA Ames Research Center, Moffett Field, California
Received 1979 July 5; accepted 1979 September 4

ABSTRACT

The dynamic collapse of rotating gas clouds is calculated for a wide range of initial conditions. Properties of cloud models are compared with observed radio and optical properties of Bok globules, to test the hypothesis that globules undergo collapse and to determine parameters which are not easily observed. Five of the six globules studied are consistent with collapse models. It is inferred that these objects have masses of about 100 $M_\odot$ and ages smaller than their free-fall times. Inferred initial densities are much larger than minimum densities for gravitational collapse, suggesting that collapse is initiated by strong external compression or that globules are fragments of larger condensed clouds. Values inferred for the $^{13}CO/H_2$ ratio are smaller than previous estimates and depend strongly on cloud density.

Subject headings: hydrodynamics — nebulae: general — stars: formation

I. INTRODUCTION

Evidence from optical and radio observations is accumulating in support of the hypothesis that the compact dark clouds known as Bok globules are undergoing gravitational collapse and may eventually form stars. The presence of macroscopic mass motions is implied by observations showing suprathermal widths for radio molecular lines. Moreover, when several molecular transitions are observed in a cloud, the line width toward the center depends on the overall size of the emitting region, suggesting that the motion is systematic and radial (Martin and Barrett 1977). Finally, the radii, densities, and temperatures derived for these objects from both star counts and molecular line studies indicate that their gravitational energy is much larger than their thermal energy, so that in the absence of additional supporting mechanisms such as rotation, magnetic fields, or turbulence, the dominant motion must be one of collapse (Dickman 1976).

Rotation can support a cloud only in the plane perpendicular to the rotation axis. Collapse will continue parallel to the rotation axis, leading to a flattened configuration. For three globules, there is observational evidence of rotation at a velocity comparable to the velocity of collapse (§ II), but for most globules rotation appears to be absent or small.

Turbulent motions large enough to support these clouds would be supersonic and subject to dissipation on a time scale shorter than the time scale of collapse. Moreover, the dissipation of turbulence would heat the gas to temperatures higher than those observed. The role of magnetic forces is more difficult to predict, and observational data are generally not available. For these reasons, and to better assess the role of rotation, turbulence and magnetic fields are not included in the present study.

Regularity in shape, isolation from other clouds,

[1] NAS/NRC Postdoctoral Research Associate.

an absence of embedded energy sources, uniform temperature, and smoothly varying density make the Bok globules attractive objects for numerical modeling. In this paper we address the question of whether the observed properties of globules are consistent with those of simple numerical models of rotating and nonrotating collapsing clouds. Such agreement would support the hypothesis that globules are collapsing protostellar objects and would allow the inference of cloud properties not directly observable, including initial conditions and probable future evolution.

In § II we summarize the available observational data and define several parameters that have proved useful in comparing observations and models. The comparison procedure is described in § III, and results for six globules are given in § IV. In § V we summarize the results and give some suggestions for further work.

II. OBSERVATIONAL DATA

The determination of dark cloud properties from star counts has been pioneered by Bok and his coworkers. A summary of methods for deriving the distance to a cloud and the absorption and mass of the dust component has been given by Bok and Cordwell (1973). It is difficult, however, to apply these statistical techniques to small, opaque globules through which few stars are seen. Frequently, the absorption is obtained only as an average over an area comparable to that of the globule, and only a minimum value is obtained if the globule is completely opaque. Lower limits to the absorption in several globule cores are given by Bok and Cordwell, and by Bok, Cordwell, and Cromwell (1971), Bok and McCarthy (1974), and Bok (1977). The spatial variation of the absorption has been measured for only a few of the largest globules: B361 has been mapped by Schmidt (1975) and several globules have been mapped by Dickman (1976).

At infrared and radio wavelengths, we see more deeply into the dusty material. Data on the infrared properties of globules are just now becoming available. Thermal emission from dust in the core of the globule B335 has been detected by Keene *et al.* (1978) at far-infrared wavelengths. From the observed spectrum, they determine the optical depth of the dust and a dust temperature of 10 K (see Table 1 and § IVc).

Microwave molecular emission lines are useful probes of the physical state and dynamics of the gas component. The most widespread and easily detectable molecules are ^{12}CO and ^{13}CO, which have been mapped in several globules by Dickman (1976), Milman (1977), and Martin and Barrett (1977). The gas kinetic temperature may be determined from the optically thick $J = 1 \rightarrow 0$ rotational transition of ^{12}CO. It is found to be ~ 10 K with only small variations from cloud to cloud or within an individual cloud. The corresponding optically thin transition of ^{13}CO provides both the projected abundance of ^{13}CO molecules and information on the velocity field. In the absence of turbulence, the ^{13}CO line width at the cloud center measures the average radial velocity of collapse (or expansion), and the variation of the line center velocity across the cloud is a measure of the rotational velocity. The observations by Milman and by Martin and Barrett indicate solid-body rotation in the cores of the globules B361, B163, and B163-SW.

A more complete picture is possible if additional molecular lines are observed. For example, from transitions of CS, NH_3, H_2CO, and OH, Martin and Barrett have determined molecular abundances and a lower limit to the total gas density in several clouds.

As with the optical observations, the radio observations do not yet warrant detailed comparison with numerical models. Many globules have been observed at the central position or along cross axes, but few have been thoroughly mapped. In addition, there are problems of resolution. The best spatial resolution with existing microwave telescopes is $1'-2'$, or about 25–50% of the average globule size, and the velocity resolution is typically 50% of the line width.

We have therefore restricted our analysis to a small number of easily measured but diagnostically useful cloud properties. Six observable parameters have been used in the model-fitting procedure. The definitions of these parameters and our estimates of the observational precision are as follows:

1. $N_{13}(0) \equiv$ the ^{13}CO column density at the center of the cloud. The largest error in N_{13} probably results from the assumption of LTE in deriving N_{13} from the antenna temperature. We estimate this error to be $\pm 50\%$, based on an analysis by Dickman (1976). The finite telescope beam size is not included as a source of error because beam smoothing has been employed in calculating N_{13} from the numerical models.

2. $R_c \equiv$ the core radius, defined as the linear distance from the center of the cloud to the point on the major axis at which the ^{13}CO column density is 50% of $N_{13}(0)$. The principal error is the uncertainty in the distance to the cloud, which we estimate to be $\pm 50\%$.

3. $Z_c/R_c \equiv$ the core axis ratio, defined as the ratio of the minor-axis and major-axis core radii. This quantity is independent of the distance to the cloud. The principal sources of error are the uncertainty in the antenna temperature and the finite spacing of observed positions. Again, we estimate the error to be $\pm 50\%$.

4. $\Delta V_{13}(0) \equiv$ the half-width at half-height of the ^{13}CO line profile at the cloud center. The uncertainty in ΔV_{13} is assumed to be 0.27 km s^{-1}, the velocity width of the filters used for the CO observations.

5. $V_{rot}(R_c) \equiv$ the rotational velocity at the edge of the core, as determined from the ^{13}CO velocity shift. The uncertainty in the measured value is assumed to be the 0.27 km s^{-1} filter width.

6. $R_{opt}/R_c \equiv$ the ratio of the optical radius to the ^{13}CO core radius. A ratio of radii is used to eliminate the uncertainty in the distance. In most cases, the optical radius has been measured as the distance between the center and the apparent edge of the globule on enlargements of Palomar red prints included in the paper by Martin and Barrett (1977). For B361, R_{opt} is obtained from the absorption profile measured by Schmidt as the distance to the point where the visual absorption is 2 mag. The uncertainty in the quantity R_{opt}/R_c is estimated to be $\pm 50\%$.

In selecting globules for comparison with numerical models, we have chosen only those which are regular in shape and well mapped in CO. We have excluded globules with multiple-component lines, which may not be single collapsing objects. If a globule has been mapped by more than one observer, the highest-resolution measurements have been used. The six globules selected for the present study are B163, B163-SW, B335, B68, ORI-I-2, and B361. Several observed properties of these clouds are given in Table 1. The quantities listed are the six model-fitting parameters defined above; the distance; the kinetic temperature, gas density, and visual extinction at the center; and the mean optical depth at 290 μm.

III. MODELS

a) The Numerical Code and Initial Conditions

Evolutionary sequences of cloud models were generated with the hydrodynamic code described by Black and Bodenheimer (1975). The calculations include gravitational collapse with axial symmetry, rotation, compressional heating, radiative transfer, and a constant surface boundary pressure.

The models are composed entirely of hydrogen, which remains in the molecular state over the ranges of temperature and density obtained. Several of the model-fitting parameters depend, however, on the distribution of the molecule ^{13}CO. For lack of more detailed information, we assume that the abundance ratio of ^{13}CO to H_2 is uniform throughout the cloud. The value of this ratio is determined for each globule by the model-fitting procedure (§ IVa).

The initial models are spherical clouds with uniform temperature, density, and angular velocity. The initial

TABLE 1
OBSERVED PROPERTIES OF GLOBULES

Parameter	B163	B163-SW	B335	B68	ORI-I-2	B361
$N_{13}(0)$	1.0E16[a]	5.5E15[a]	1.0E16[a]	3.5E15[a]	1.2E16[a]	7.3E15[b]
R_c (cm)	7.7E17[a]	4.9E17[a]	8.1E17[a]	4.1E17[a]	4.0E17[a]	1.2E18[b]
Z_c/R_c	0.6[a]	0.7[a]	0.8[a]	0.6[a]	0.7[a]	0.8[i]
$V_{13}(0)$ (km s^{-1})	0.5[a]	0.5[a]	0.4[a]	0.5[a]	0.75[a]	2.0[b]
$V_{rot}(R_c)$ (km s^{-1})	0.45[a]	0.5[a]	0[a]	0[a]	0[a]	1.2[b]
R_{opt}/R_c	1.2[a]	1.3[a]	1.1[a]	1.1[a]	1.1[a]	1.3[d]
Distance (pc)	400[a,i]	400[a,i]	400[f]	200[f]	400[e]	350[c]
$T_K(0)$ (K)	9[a]	9[a]	10[a]	11[a]	19[a]	8.5[b]
n_0 (cm^{-3})	...	...	≥ 1.4E4[a]	≥ 8.0E3[a]	≥ 2.9E4[a]	...
$A_v(0)$ (mag)	≥ 8[a,i]	≥ 8[a,i]	≥ 10[f]	≥ 25[g]	≥ 8[e]	≥ 7[c]
$\langle T_{290\mu m}\rangle$	...	...	0.02[h]	...	...	...

[a] Martin and Barrett 1977.
[b] Milman 1977.
[c] Schmidt 1975.
[d] R_{opt} from Schmidt 1975; R_c from Milman 1977.
[e] Bok, Cordwell, and Cromwell 1971.
[f] Bok and McCarthy 1974.
[g] Bok 1977.
[h] Keene *et al.* 1978.
[i] Not measured, estimate given.

temperature is in each case taken to be 10 K, but sequences are calculated for a wide range of density and angular velocity, including nonrotating clouds. A particular evolutionary sequence is defined by the values of three parameters: the total mass M, the initial ratio α of the thermal energy to the gravitational energy, and the initial ratio β of the rotational energy to the gravitational energy.

The calculations were made for a mass of 1000 $M_\odot$, but because the models remain isothermal, the results may be scaled to other masses (Bodenheimer and Black 1978).[2] Black and Bodenheimer (1976) show that a sustained collapse is possible only if $\alpha \leq (1 - 1.43\beta)$. Sequences satisfying this relation have been calculated for 15 combinations of α and β corresponding to $\alpha = 0.05, 0.16$, and 0.5 and $\beta = 0.0$, 0.005, 0.02, 0.08, and 0.32. Two additional sequences calculated for $\alpha = 1.6$ and $\beta = 0.0$ and 0.02 showed an initial collapse followed by expansion.

The initial conditions may also be expressed as the total mass M, the hydrogen molecule density n_i, and the angular velocity ω_i. In terms of the α and β parameters,

$$n_i = 0.42 \left(\frac{\alpha}{0.5}\right)^{-3} \left(\frac{M}{1000\,M_\odot}\right)^{-2} \text{cm}^{-3} \qquad (1)$$

$$\omega_i = 1.6 \times 10^{-16} \left(\frac{\alpha}{0.5}\right)^{-3/2} \left(\frac{\beta}{0.02}\right)^{1/2} \left(\frac{M}{1000\,M_\odot}\right)^{-1} \text{s}^{-1} \qquad (2)$$

b) Characteristics of the Evolution

Numerical calculations of the collapse of rotating and nonrotating clouds have been described by several

[2] The results could also be scaled to represent values of temperature and mean molecular weight other than the values $T = 10$ K and $\mu = 2$ used for the calculations.

authors (see, e.g., review papers by Larson 1973 and Bodenheimer and Black 1978). As models calculated with the present code have been described in detail by Black and Bodenheimer (1976), we summarize here only the principal features of the evolution.

In both rotating and nonrotating sequences, the collapse proceeds most rapidly at the center of the cloud in a small core of nearly uniform density. Outside of the core, the density falls off as r^{-2}, where r is the distance to the center. During the initial phase of the collapse the infall velocity increases linearly with r. However, at a still early time the velocity distribution becomes nonmonotonic, and in an outer region containing a significant fraction of the cloud mass, the velocity falls off approximately as $r^{-1/2}$. The magnitude of the infall velocity is greatest for the sequences with the smallest initial α.

When rotation is present, the collapse is retarded in the direction perpendicular to the rotation axis, and the density contours become flattened. The high-density core continues to rotate nearly as a solid body, but the angular velocity of material outside the core falls off approximately as $r^{-3/2}$. The asymmetry of the velocity field and the rate of flattening are largest for the sequences of largest initial β, but after about one free-fall time, all rotating models have flattened to thin disks. Within this flattened configuration, most investigators find that an off-center density maximum (i.e., a ring) develops as rotation slows the collapse and material begins to flow outward. The ring grows in mass and eventually collapses under self-gravity. The present calculations are terminated at the stage of ring collapse. Throughout the calculated evolution, the models remain optically thin and isothermal at the initial temperature.

The above behavior is shown by all sequences except those with $\alpha = 1.6$, in which the initial models

violate the condition for sustained collapse. These sequences undergo an initial collapse, followed by a "bounce" and expansion toward the original state.

IV. COMPARISON OF OBSERVATIONS AND MODELS

a) Method of Comparison

A particular model may be specified by the quantities α, β, and M, which define the evolutionary sequence, and by the evolutionary time t. To derive observable properties, we must also specify the inclination i of the rotation axis to the plane of the sky. The fitting parameters defined in § II have been calculated for a five-dimensional array of models determined by the set of discrete values of α and β, a set of masses between 10 and 10^4 $M_\odot$, a set of inclination angles between $0°$ and $90°$, and a sequence of evolutionary times. The calculation of the fitting parameters is described in Appendix A.

The following procedure has been used to compare models and observational data. For each globule, we first select from the above-defined array all models which represent the five parameters R_c, Z_c/R_c, $\Delta V_{13}(0)$, $V_{rot}(R_c)$, and R_{opt}/R_c within the estimated observational uncertainty. From these we select as the "best-fit" model, that model for which the mean-square relative error in the fitting parameters is a minimum. From the best-fit model and the range of models fitting the observations, we may determine the most likely value and the range of uncertainty of any other physical quantity. In particular, the hydrogen column density of the models has been used with the sixth observed parameter $N_{13}(0)$ to establish the best value and the range of the abundance ratio $^{13}CO/H_2$.

b) General Properties of the Best-Fit Models

For five of the six globules studied, we have obtained numerical models consistent with the observations. The globule B361 could not be fitted, principally because of the large line width (see § IVc). The other globules have been matched to models from sequences with $\alpha \leq 0.5$, which undergo sustained collapse. None of the globules is consistent with models of the larger α sequences, which undergo an eventual bounce and expansion.

Some inferred properties of the successfully matched globules are given in Table 2. Table 2A lists for each globule the best value and the range of uncertainty of the parameters α, β, M, i, $^{13}CO/H_2$, and t. Corresponding values for the initial density and angular velocity are listed in Table 2B, together with the central density, maximum density, visual extinction, and far-infrared optical depth, which may be compared with observed values given in Table 1. There is a large uncertainty in the derived properties of each globule because of the large observational uncertainty in the model-fitting parameters.[3] Nevertheless, if we

consider only the best-fit models, then the five globules have similar properties, which may be summarized as follows:

Mass.—The total mass of an individual globule is predicted to be between 53 and 170 $M_\odot$. Between 40% and 60% of the mass is *outside* of the core and would not be detected in CO at the sensitivity of currently available instruments.

Initial conditions.—The initial density is predicted to be a factor of 10^2–10^4 larger than the minimum density for collapse. This result has important implications for our understanding of the conditions that initiate collapse. It is consistent, for example, with scenarios in which the globule is strongly compressed prior to collapse or in which the globule is a fragment of a more massive collapsing cloud.

The predicted initial angular velocities range between 0 and 3×10^{-14} s^{-1}. It would therefore appear that some globules have evolved from clouds with angular velocities smaller than the local galactic angular velocity of 10^{-15} s^{-1}, commonly assumed to be a lower limit for the rotation rate of interstellar clouds. It must be noted, though, that these globules have best-fit models belonging to the $\alpha = 0.05$, $\beta = 0$ sequence for which the initial angular velocity ω_i is zero, and that models of similar mass belonging to the $\alpha = 0.05$, $\beta = 0.005$ sequence have $\omega_i > 10^{-14}$ s^{-1}. Thus we cannot actually exclude rotation rates of 10^{-15} s^{-1}, and the initial angular velocity of each globule studied may be consistent with this lower limit.

Age.—The ages predicted for these globules are between 10^5 and 10^6 yr. This is only 50–90% of the free-fall time, and the cloud model has not yet formed a ring. Flattening to a thin disk and ring formation occur rapidly at about one free-fall time. The rate of flattening depends on α and β, but, as an average, axis ratios smaller than 0.5 occur only during the last 5% of the evolution calculated. As the subsequent evolution should occur on an even shorter time scale, *we would expect to observe few highly flattened globules.*

Central density and visual extinction.—Predicted central densities range between 10^4 and 2×10^5 hydrogen molecules per cm^3, consistent with the observational lower limits given in Table 1. Predicted values of the central visual extinction range between 28 and 140 mag and are considerably larger than measured lower limits.

^{13}CO *to* H_2 *abundance ratio.*—The values predicted for the $^{13}CO/H_2$ ratio are 8–70 times smaller than the value 2×10^{-6} derived by Dickman (1976) from observations of less dense clouds. In Figure 1, the ratio $^{13}CO/H_2$ is plotted for each globule as a function of the central density. *It is evident that there is a systematic relationship, with the smallest values of $^{13}CO/H_2$ corresponding to the densest clouds.* Also shown are results obtained by Wootten *et al.* (1978) for a variety of molecular clouds observed in CO and H_2CO. None of the globules which we have modeled is included, and the densities are obtained from the H_2CO data—a procedure entirely independent of our

---

[3] If the error limits on the fitting parameters are arbitrarily reduced, the range of models shrinks accordingly. Thus a unique model could be obtained if these parameters were accurately measured.

TABLE 2A

DERIVED PROPERTIES OF GLOBULES[a]

Globule	α	β	$M/M_\odot$	i (deg)[b]	$^{13}CO/H_2$	t (yr)	t/t_{ff}[c]
B163...........	0.16 (0.16–0.5)	0.08 (0.02–0.32)	99 (32–490)	0 (0–60)	2.6E−7 (6.9E−8–1.3E−6)	8.7E5 (2.0E5–2.9E7)	0.92 (0.59–1.3)
B163-SW........	0.16 (0.05–0.5)	0.08 (0.02–0.32)	53 (10–210)	30 (0–60)	1.2E−7 (1.2E−8–1.8E−6)	4.5E5 (2.9E4–1.1E6)	0.87 (0.28–1.4)
B335...........	0.05 (0.05–0.5)	0 (0–0.32)	170 (10–610)	... (0–90)	2.0E−7 (3.1E−8–4.4E−6)	1.6E5 (2.3E4–3.6E7)	0.52 (0.15–1.5)
B68...........	0.05 (0.05–0.5)	0 (0–0.32)	98 (18–180)	... (0–60)	2.8E−8 (5.4E−9–29.E−7)	1.0E5 (2.4E4–3.0E6)	0.55 (0.30–1.5)
ORI-I-2........	0.05 (0.05–0.5)	0 (0–0.32)	130 (10–250)	... (0–90)	6.9E−8 (1.2E−8–4.1E−6)	1.8E5 (6.2E4–8.3E5)	0.75 (0.50–1.4)

[a] For each globule, the first line refers to the best-fit model, and the second line refers to the range of models within the observational uncertainty.
[b] Defined only for models with $\beta > 0$.
[c] Age relative to the free-fall time.

TABLE 2B

DERIVED PROPERTIES OF GLOBULES[a]

Globule	n_i (cm^{-3})	ω_i (s^{-1})	n_0 (cm^{-3})	n_{max} (cm^{-3})	$A_v(0)$ (mag)	$\langle \tau_{290\mu m} \rangle$
B163...........	1.5E3 (1.7–1.4E4)	1.9E−14 (3.3E−16–1.2E−13)	1.7E4 (7.0E3–5.8E6)	1.7E4 (7.0E3–6.3E6)	28 (9–52)	1.3E−2 (4.1E−3–2.8E−2)
B163-SW........	5.0E3 (1.1E3–3.3E5)	3.5E−14 (1.6E−14–5.7E−13)	4.6E4 (2.1E4–1.3E7)	4.6E4 (2.1E4–5.0E8)	36 (4–180)	2.0E−2 (1.1E−3–1.0E−1)
B335...........	1.4E4 (1.1–8.7E4)	0 (0–2.9E−13)	2.8E4 (1.3E3–2.5E6)	2.8E4 (1.3E3–1.1E7)	41 (3–130)	2.1E−2 (8.4E−4–6.9E−2)
B68...........	4.3E4 (1.3E2–2.7E5)	0 (0–2.0E−13)	1.1E5 (2.2E4–2.9E6)	1.1E5 (2.2E4–3.2E6)	98 (15–260)	4.2E−2 (8.0E−3–1.4E−1)
ORI-I-2........	2.4E4 (2.7E3–5.2E5)	0 (0–7.2E−13)	2.0E5 (3.9E4–6.6E8)	2.0E5 (3.9E4–2.2E10)	140 (4–390)	5.5E−2 (1.4E−2–2.1E−1)

[a] For each globule, the first line refers to the best-fit model, and the second line refers to the range of models within the observational uncertainty.

own. Nevertheless, the relationship between $^{13}CO/H_2$ and density derived by Wootten *et al.* is seen to be consistent with that derived from our models. This result is of considerable importance because cloud masses are often estimated from ^{13}CO measurements and an arbitrary value for the ratio $^{13}CO/H_2$. It appears that the use of Dickman's value will underestimate the density and total mass of clouds in which $n(H_2) \gtrsim 10^3 \text{ cm}^{-3}$.

The observed abundances shown in Figure 1 represent mean values along the line of sight. The variation of the mean $^{13}CO/H_2$ ratio with the central density from cloud to cloud suggests that this ratio may vary with local density within individual clouds.

To estimate the magnitude of the local ^{13}CO abundance variation, we have applied a relationship of the form

$$\frac{n(^{13}CO)}{n(H_2)} = 2 \times 10^{-6} \quad \text{for } n(H_2) \leq 10^3 \text{ cm}^{-3},$$

$$= \frac{2 \times 10^{-6}}{[n(H_2)/10^3 \text{ cm}^{-3}]^p} \quad \text{for } n(H_2) > 10^3 \text{ cm}^{-3}, \tag{3}$$

to the models given in Table 2. These models match the observed ^{13}CO column densities for $0.7 \lesssim p \lesssim 0.9$. To test the effect of a varying ^{13}CO abundance on the selection of best-fit models, we then fitted the globules B335 and Ori-I-2 with models for which the $^{13}CO/H_2$ ratio is given by equation (3) with $p = 1$. The derived globule parameters are shown in Table 3 together with the parameters for models of uniform abundance ($p = 0$). It is seen that the values derived for α and β are the same in the two cases, but that densities differ by as much as a factor of 3 and other parameters differ by as much as a factor of 2. We conclude that ^{13}CO abundance variations may affect the derived globule properties and that effort should be directed toward measuring variations within individual clouds. However, the qualitative conclusions of this paper are not affected by abundance variations of the magnitude considered here, and comparison of Table 2 and
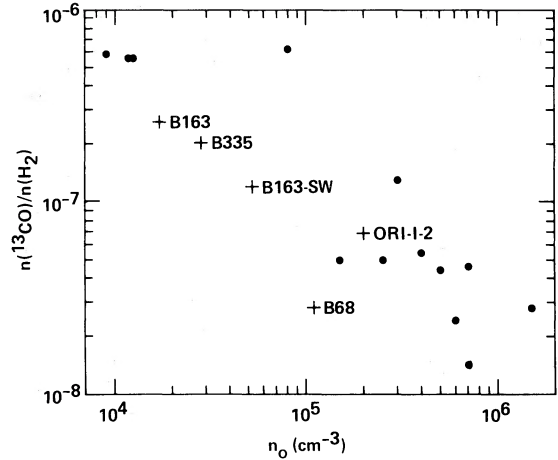

FIG. 1.—Abundance ratio $^{13}CO/H_2$ versus total gas density at center of cloud. *Dots*, measurements of a variety of molecular clouds by Wootten *et al.* (1978). *Plus signs*, our best-fit globule models.

Table 3 shows the effects of a varying rather than a uniform ^{13}CO abundance to be smaller than the effects of observational uncertainty in the model-fitting parameters.

c) Properties of Individual Globules

i) B163 and B163-SW

These two globules appear to be physically related. Each is elongated in the direction of the galactic plane and each has a projected rotation axis directed opposite to that of the galaxy. The pair also exhibits relative orbital motion, with the orbital angular momentum aligned with the direction of rotation. These alignments have led Martin and Barrett (1977) to suggest that the globules were formed by the contraction and fragmentation of a larger cloud, with an angular momentum due to differential galactic rotation. Such an origin is consistent with the physical properties derived in the present study. The model ages derived independently for the two globules agree

TABLE 3

DERIVED GLOBULE PROPERTIES FOR $n(^{13}CO)/n(H_2) \propto n(H_2)^{-p}$

Globule	α	β	$M/M_\odot$	$N(^{13}CO)/N(H_2)$	t (yr)	t_{ff}
B335 ($p = 0$)	0.05	0	170	2.0E − 7	1.6E5	0.52
B335 ($p = 1$)	0.05	0	145	2.5E − 7	1.2E5	0.45
ORI-I-2 ($p = 0$)	0.05	0	130	6.9E − 8	1.8E5	0.75
ORI-I-2 ($p = 1$)	0.05	0	72	1.5E − 7	9.1E4	0.71

Globule	n_i (cm^{-3})	ω_i (s^{-1})	n_0 (cm^{-3})	$A_v(0)$ (mag)	$\langle \tau_{290\mu m} \rangle$
B335 ($p = 0$)	1.4E4	0	2.8E4	41	2.1E − 2
B335 ($p = 1$)	2.0E4	0	3.5E4	32	1.6E − 2
ORI-I-2 ($p = 0$)	2.4E4	0	2.0E5	140	5.5E − 2
ORI-I-2 ($p = 1$)	8.1E4	0	5.0E5	65	2.5E − 2

to within a factor of 2, which is smaller than the expected error in either value. Also, similar values are derived for the density and the angular velocity which characterize the initial conditions for each globule.

Martin and Barrett observe maxima in the CO emission at two points along the major axis of the globule B163. These observations suggest a ring-shaped cloud viewed edge-on, but, as the authors point out, they may also reflect the poorer ratio of signal to noise at the cloud's outer boundary. We are unable to substantiate the suggestion of a ringlike shape for this cloud. Our best-fit model for B163 does not have a ring. Several models yielding poorer although still acceptable fits to the basic parameters do have rings, but the ring properties do not match the observed structure.

ii) B335

This is the only globule for which measurements of infrared emission are available. We have assumed that the emission is thermal radiation from dust and have compared the observed flux with the flux calculated from our best-fit model.

The flux from the 2′ diameter central core of B335 has been measured by Keene et al. (1978) at wavelengths between 175 and 450 μm. At these wavelengths the cloud is optically thin, and the flux is proportional to the optical depth. If the spectrum is fitted with a Planck function and a $(1/\lambda)^2$ opacity law, the best fit is for a temperature of 10 K and an optical depth of 0.02 at the 290 μm emission peak.

Our best-fit model for B335 has a temperature of 10 K, consistent with the observed temperatures of the dust and the gas. The optical depth at positions in the model has been calculated from the gas density and estimated values for the dust/gas ratio and the dust opacity. (The details of this calculation are given in Appendix B.) The average optical depth in the 2′ core is 0.021, in excellent agreement with the observed value. This agreement enhances our confidence in the other derived properties of the globule.

iii) B68 and ORI-I-2

These are the densest of the globules which we have modeled. At 290 μm, the best-fit models have optical depths of 0.04 and 0.05. As a result, the far-infrared flux is predicted to be about twice that measured for B335. Each of these objects should therefore be well-suited for observations which could either substantiate the physical picture advanced here or point the way toward a different concept.

iv) B361

None of the theoretical models can explain all of the observed properties of B361. The ^{13}CO line width is much larger than line widths in the other globules which we have modeled. Collapse velocities consistent with the observed line width occur in models of the $\alpha = 0.05$ sequences at times near the end of the calculated evolution, but these models are inconsistent with other observed properties. The failure of the models to match the observations may indicate that B361 is not a single collapsing object or that turbulent motion contributes to the line width.

V. SUMMARY AND SUGGESTIONS FOR FURTHER WORK

From a comparison of globule observations and numerical models, we have reached the following conclusions:

1. Five of the six globules studied can be fitted to dynamic cloud models. Because of large observational uncertainty in the fitting parameters, each globule has a wide range of acceptable models. However, this range includes only models which are gravitationally unstable and undergoing collapse.

2. From the best-fit models, we have derived globule properties which are not readily observed. The derived masses are of the order of 100 $M_\odot$. The ages are smaller than one free-fall time, and no globule has reached the stage of rapid flattening and ring formation. Inferred initial densities are much larger than minimum densities for gravitational instability, suggesting that collapse is initiated by strong external compression or that the globules are fragments of larger condensed clouds. Similar properties derived for the pair of globules B163 and B163-SW support the view that they are associated cloud fragments.

3. The ^{13}CO/H$_2$ ratio is predicted to be an order of magnitude or more smaller in globules than in less dense clouds. The values derived for ^{13}CO/H$_2$ show a systematic dependence on the total gas density, in agreement with observational results for other dense molecular clouds.

4. Other properties of the cloud models are suitable to further observational test. Far-infrared observations of B335 are consistent with model predictions, but corresponding observations for the other globules modeled are not yet available.

Although the present findings suggest that most Bok globules are collapsing, this conclusion should be re-examined with improvements in both observations and theoretical models. Detailed line profiles are now being calculated for the models reported here, but the effort is limited by an incomplete understanding of the molecular chemistry. It would be most useful to have a numerical scheme for the chemical reactions which would include all major observable molecules and yet be simple enough for use with an evolutionary code. In addition, the effects of magnetic fields and turbulence and of alternative initial conditions remain to be explored.

The most urgent need, however, is for additional and more detailed observations. A larger number of globules should be observed at visual, infrared, and radio wavelengths. Complete mappings would be more useful than observations at a few isolated positions, and measurements should have the highest possible spatial and velocity resolution.

APPENDIX A

CALCULATION OF THE MODEL-FITTING PARAMETERS

The derivation of six model-fitting parameters from the globule observations was described in § II. This appendix describes how the same parameters are derived from the numerical models.

The parameter $N_{13}(0)$ is calculated as the product of the H_2 column density and the $^{13}CO/H_2$ abundance ratio at the center of the model. The parameters R_c and Z_c/R_c are calculated from the gradient of the H_2 column density, under the assumption that the $^{13}CO/H_2$ ratio is constant. For each of these calculations, the model column densities are smoothed so as to approximate the beam-smoothing of the observations. Dickman (1976) has shown that to sufficient accuracy we may evaluate the smoothed column density $\langle N_{H_2} \rangle$ as

$$\langle N_{H_2} \rangle = \frac{\iint_{\text{beam}} N_{H_2}(x, y) P(x, y) \, dx \, dy}{\iint_{\text{beam}} P(x, y) \, dx \, dy} \, , \tag{A1}$$

where x and y are rectangular coordinates of points in the model and $P(x, y)$ is the telescope beam pattern. We have approximated the beam pattern by taking $P = 1$ at points within the half-power width and $P = 0$ elsewhere.

The line width ΔV_{13} is estimated from the models as the mass-averaged velocity along the line of sight. To form this average, the absolute value of the projected velocity (including both collapse and rotation) is weighted by the local density. For the model-fitting, we require only $\Delta V_{13}(0)$, the line width at the center of the globule. Although only collapse motions contribute to the line width calculated at the center, both collapse and rotation contribute to the line width measured with a finite telescope beam. To approximate the effect of beam-smoothing, we average ΔV_{13} over positions near the center in the same manner as we average the column density (eq. [A1]). As ΔV_{13} varies slowly with position, this average should be sufficiently accurate for the present application.

It is not obvious that the value calculated for $\Delta V_{13}(0)$ may be compared with the observed width of the ^{13}CO line profile. However, we have constructed approximate line profiles for several models, neglecting self-absorption and using power laws for the density and velocity, and we find that the widths of these profiles differ from the mass-averaged velocity by at most 30%. This error is smaller than the typical velocity resolution of the observations.

The quantity V_{rot} is calculated as the maximum projected rotational velocity along the line of sight. For the fitting parameter $V_{\text{rot}}(R_c)$, we again use a beam-averaged velocity, determined from the appropriate analog of equation (A1).

The optical radius R_{opt} is determined as the distance between the center of the model and the point on the major axis at which the visual extinction is 2 mag. The extinction is derived from the H_2 column density as

$$A_v \, (\text{mag}) = N_{H_2} \, (\text{cm}^{-2})/1.25 \times 10^{21} \tag{A2}$$

(Jenkins and Savage 1974). For the calculation of A_v the column density is not beam-smoothed. However, the beam-smoothed core radius is used to form the model-fitting parameter R_{opt}/R_c.

APPENDIX B

CALCULATION OF THE INFRARED EMISSION

For an optically thin, isothermal cloud, the flux measured at wavelength λ is

$$F_\lambda = B(\lambda, T)\langle \tau_\lambda \rangle \Delta\omega \, , \tag{B1}$$

where $B(\lambda, T)$ is the Planck function for temperature T, $\Delta\omega$ is the angular size of the telescope beam, and $\langle \tau_\lambda \rangle$ is the optical depth averaged over the angle $\Delta\omega$:

$$\langle \tau_\lambda \rangle = \frac{\int_{\Delta\omega} \tau_\lambda \, d\omega}{\Delta\omega} \, . \tag{B2}$$

Along any line of sight through the cloud, τ_λ is given by

$$\tau_\lambda = \pi a^2 Q_\lambda \int n_g \, ds \, , \tag{B3}$$

where a is the average radius of a dust grain, n_g is the number density of grains, Q_λ is the absorption efficiency, and s is the path length. If we let p be the mass fraction of dust relative to hydrogen, then equation (B3) may be written as

$$\tau_\lambda = \frac{3 Q_\lambda p m_{H_2} N_{H_2}}{4 a \rho_g} \, , \tag{B4}$$

where ρ_g is the density of a dust grain, m_{H_2} is the mass of an H_2 molecule, and N_{H_2} is the H_2 column density.

Equation (B4) has been used to calculate τ_λ from the models. We have taken $p = 0.01$ and have used values of $a = 0.05 \, \mu\text{m}$, $\rho_g = 2 \, \text{g cm}^{-3}$, and $Q_\lambda = 16/\lambda(\mu\text{m})^2$ appropriate to ice-coated silicate grains (Knacke 1979). The optical depth of each globule at 290 μm is given in Table 2B. The values listed have been averaged over the 2' diameter central core of the best-fit models. Predicted values for the flux at 290 μm may be determined from equation (B1), with $T = 10$ K.

REFERENCES

Black, D. C., and Bodenheimer, P. 1975, *Ap. J.*, **199**, 619.
———. 1976, *Ap. J.*, **206**, 138.
Bodenheimer, P., and Black, D. C. 1978, in *Protostars and Planets*, ed. T. Gehrels (Tucson: University of Arizona Press), p. 288.
Bok, B. J. 1977, *Pub. A.S.P.*, **89**, 597.
Bok, B. J., and Cordwell, C. S. 1973, in *Molecules in the Galactic Environment*, ed. M. A. Gordon and L. E. Snyder (New York: Wiley), p. 53.
Bok, B. J., Cordwell, C. S., and Cromwell, R. H. 1971, in *Dark Nebulae, Globules, and Protostars*, ed. B. T. Lynds (Tucson: University of Arizona Press), p. 33.
Bok, B. J., and McCarthy, C. C. 1974, *A.J.*, **79**, 42.
Dickman, R. L. 1976, Ph.D. thesis, Columbia University.
Jenkins, E. B., and Savage, B. D. 1974, *Ap. J.*, **187**, 243.
Keene, J., Harper, D. A., Hildebrand, R. H., Lowenstein, R. F., Moseley, S. H., Whitcomb, S. E., and Winston, R. 1978, *Bull. AAS.*, **10**, 687.
Knacke, R. F. 1979, private communication.
Larson, R. B. 1973, *Fundamentals of Cosmic Phys.*, **1**, 1.
Martin, R. N., and Barrett, A. H. 1977, *M.I.T. Radio Astronomy Contributions*, No. 3.
Milman, A. S. 1977, *Ap. J.*, **211**, 128.
Schmidt, E. G. 1975, *M.N.R.A.S.*, **172**, 401.
Wootten, A., Evans, N. J., Snell, R., and Vanden Bout, P. 1978, *Ap. J. (Letters)*, **225**, L143.

DAVID C. BLACK and KAREN R. VILLERE: Space Science Division, MS 245-3, NASA Ames Research Center, Moffett Field, CA 94035